Self-Diffusion and Tracer Diffusion of Solutions of Flexible Polymer Chains: A Comparison of Experimental Results with Theoretical Predictions

Bo Nyström* and Jaan Roots

Department of Chemistry, The University of Oslo, P.O. Box 1033, Blindern, 0315 Oslo 3, Norway

Received February 7, 1990; Revised Manuscript Received May 16, 1990

ABSTRACT: In this study literature data on the self-diffusion coefficient, D_s, of polystyrene in good solvents are analyzed with the aid of the Hess theory together with renormalization group results for the entanglement parameter. A univeral plot of the form D_s/D_0 versus X, where X is an experimentally accessible reduced concentration variable and D_0 is the self-diffusion coefficient at infinite dilution, is utilized. From the model, explicit analytical functions, without any adjustable parameter, emerge. The theoretical expressions qualitatively describe the experimental results. The tracer diffusion behavior of labeled chains in ternary solutions of compatible or slightly incompatible polymers is analyzed in the framework of a model analogous to that developed for self-diffusion. The concentration and molecular weight dependences of the tracer diffusion coefficient are qualitatively explained by the analytical functions, without any adjustable parameter, emerging from the theoretical model.

Introduction

Cooperative transport properties, such as sedimentation and translational diffusion, of polymer molecules in semidilute and concentrated solutions are governed by a mechanism where all the polymer chains are more or less collectively moving[1] in a viscous medium, so that any disentanglement or large-scale motion of each chain will not be required during the process of motion. For this type of transport phenomena, it is assumed that the gradual screening[2-4] of both hydrodynamic and excluded-volume interactions plays an important role, whereas the entanglements present should not be crucial for the process. Recent sedimentation[5,6] and mutual diffusion[7] studies seem to support this hypothesis.

On the other hand, if we consider the transport of a single chain, which has to find its way through a maze created by other chains, it can be anticipated that chain connectivity and accordingly entanglements should be momentous for the process. Previously, this type of motion has been interpreted by visualizing each chain as being confined in an effective "tube" made of all topological constraints imposed on one chain by its neighbors. Since the chains cannot cross each other, each chain can only slide or "reptate" in a snakelike motion along its tube, while any large-scale motion perpendicular to its local direction is hampered. Most of the previous theoretical approaches[1,2,8,9] were formulated in terms of phenomenological scaling laws, which give only a qualitative feature of the parameter dependence.

Recently, Hess elaborated an attractive self-consistent microscopic many-body theory yielding explicit functional forms for the calculation of self-diffusion, D_s,[10] and tracer diffusion, D_t,[11] coefficients of polymers in solution. In this theory Hess has applied the Zwanzig–Mori operator technique for generalized hydrodynamics to entangled polymer solutions. In this approach each chain interacts with its neighbor through excluded-volume interactions that are invariant under curvilinear displacements. According to our knowledge, these theoretical predictions have not been tested systematically in comparison with experimental results. Furthermore, a unitary definition of D_s and D_t does not seem to have been established in the literature. In the present study a clear distinction between these quantities is made. The notion of self-diffusion refers to the Brownian motion of one labeled-chain immersed in a unimodal solution of chemically identical chains of the same length as the test chain, while tracer diffusion denotes the diffusion of one tracer chain in a matrix where all the chains have the same polymerization index, n_m, which is different from that, n_t, of the probe. In this latter case the tracer and the matrix may originate from the same polymer or, as is more usual, from chemically unlike polymer species.

It is noteworthy that the models of Hess have been advanced without a priori resorting to the "reptation" or "tube" concept. However, it has been argued[12,13] that many of the technical simplifications introduced by Hess in the calculation of the dynamic friction function are guided by preconceived ideas of reptation.

In this work a large body of self-diffusion data reported for polystyrene in good solvents is analyzed in the framework of the theory of Hess. The analogous model developed[11] to theoretically describe the concentration and molecular weight dependences of the tracer diffusion coefficient in ternary polymer solutions is also scrutinized. The aim is to examine whether or not the experimental self-diffusion and tracer diffusion results can be rationalized within the framework of the constructed models and to make direct comparisons between the experimental results and the theoretical predictions, derived in the form of closed analytical expressions without any adjustable parameter.

Theoretical Considerations

Let us first briefly recapitulate the essential features of Hess[10,11] theory. Starting from a Fokker–Planck equation for the phase space distribution function of polymer segments, Hess elaborated a microscopic and self-consistent-field theory for the calculation of the self-diffusion coefficient of a flexible polymer chain in solutions of homogeneous polymers. In this approach the coupling between the curvilinear and the lateral motions is calculated to first-order through the concentration-dependent single-segment friction coefficient for center-of-mass motion. In this context, the curvilinear motion represents the large-scale motion along the polymer chain axis and the lateral motion acts perpendicular to the same axis. The existence of a transition to a reptation-like mode in self-diffusion is recognized at a critical segment concentration or chain length, where the perpendicular degrees

0024-9297/91/2224-0184$02.50/0

of freedom freeze in, and the curvilinear response function depicts the motion of a free Rouse chain. The conjecture is that the lateral motion is gradually hampered with increasing matrix concentration due to excluded-volume interactions; at a critical strength of interactions the lateral mobility ceases and the only mechanism left over is curvilinear motion, or reptation in conventional terminology. It is the basic assumption of the theory that repulsive forces are responsible for reptation phenomena in entangled solutions.

Recently, it was demonstrated[11] that an extension of the theory to the problem of tracer diffusion in a matrix with different molecular weight than the probe molecule is straightforward, and the main constituents of the theoretical model are intact.

Self-Diffusion. The self-diffusion process in unimodal polymer solutions is described in terms of two variables, viz., the concentration-dependent single-segment friction coefficient, $\zeta(c)$, and $\psi(c,n)$, the entanglement parameter. The final expression for the self-diffusion coefficient, D_s, reads as[10]

$$D_s/D_0 = \begin{cases} 1 - 2\psi/3 & \text{for } 0 \le \psi \le 1 \quad (1a) \\ 1/(1 + 2\psi) & \text{for } 1 \le \psi \quad (1b) \end{cases}$$

Here D_0 ($\equiv k_B T/n\zeta$) is the self-diffusion coefficient of the model Rouse chain without topological constraints. The quantity n is the polymerization index of the polymer, k_B is the Boltzmann constant, and T is the absolute temperature. For small values of ψ ($\psi \ll 1$) a Rouse-like behavior is observed. When $\psi \to 1$, lateral motion gradually freezes in, and at larger ψ-values the test chain moves predominantly by curvilinear motion, that is, reptation.

Entanglement Concept and the Free-Energy Density. Since the ψ-parameter is a basic concept and of crucial importance for a quantitative description of both self-diffusion and tracer diffusion behavior, it is appropriate to discuss this quantity separately. The principal objective of this section is to develop analytical functions, through the free-energy density variable, ΔF, for the calculation of the entanglement parameter in terms of experimentally accessible quantities. ψ is defined in terms of the mean interaction energy of one polymer chain and is proportional to its number of entanglements. This parameter may be expressed as

$$\psi \equiv n/n_c = n\Delta F/2c_s k_B T = M\Delta F/2cRT \quad (2)$$

where n_c is the critical polymerization index, at which the reptation transition takes place, c_s is the segment number concentration, c is the mass concentration (mass/volume), M is the molecular weight of the polymer, and R is the gas constant. The variable $\Delta F(c)$ represents the excluded-volume interaction contribution to the free-energy density. In order to calculate ψ, it is convenient to express the free energy in terms of the osmotic pressure, Π, which is an experimentally measurable quantity. The osmotic pressure is related to ΔF by the general formula

$$\Pi = c^2 \frac{\partial}{\partial c}\left(\frac{\Delta F}{c}\right) = c\left(\frac{\partial \Delta F}{\partial c}\right) - \Delta F \quad (3)$$

This equation may be rewritten on the following explicit form for ΔF:

$$\frac{\Delta F}{c} = \int \frac{\Pi}{c^2}\, dc \quad (4)$$

Recently, Oono and Baldwin[14] elaborated in the framework of the conformation space renormalization group theory with the aid of the ϵ-expansion method up to order $\epsilon = 4 - d$, d being the spatial dimensionality, an explicit functional form for the reduced osmotic pressure in terms of a dimensionless static scaling variable $X_{(1)}$

$$(M/RT)(\Pi/c) = 1 + (X_{(1)}/2)\exp\left\{\frac{\epsilon}{4}\frac{Z}{1+Z}\left[\frac{\mu^2}{X_{(1)}^2}\ln(\mu) + \left(1 - \frac{\mu^2}{X_{(1)}^2}\right)\ln(\mu + X_{(1)}) + \frac{\mu}{X_{(1)}}\right]\right\} \quad (5)$$

where $\mu \equiv M_n/M_w$ is a polydispersity parameter. $X_{(1)}$ is a parameter proportional to c/c_a, where c_a is the overlap threshold concentration, or may be related to the second virial coefficient, A_2, by

$$A_2 Mc = X_{(1)}\left[\frac{8 + 9Z}{16(1+Z)} - \frac{\epsilon}{8}\ln(1/\mu)\right] \quad (6)$$

where Z is an interaction variable, which simulates the crossover between Gaussian (Θ) ($Z \to 0$) and self-avoiding or good-solvent ($Z \to \infty$) limits. In the limit $Z \to \infty$ the expression, originally derived by Ohta and Oono,[15] is recovered:

$$(M/RT)(\Pi/c) = 1 + (X_{(1)}/2)\exp\left\{\frac{\epsilon}{4}\left[\frac{\mu^2}{X_{(1)}^2}\ln(\mu) + \left(1 - \frac{\mu^2}{X_{(1)}^2}\right)\ln(\mu + X_{(1)}) + \frac{\mu}{X_{(1)}}\right]\right\} \quad (5a)$$

$$A_2 Mc = X_{(1)}\left(\frac{9}{16} - \frac{\epsilon}{8}\ln(1/\mu)\right) \quad (6a)$$

It has been shown that the polydispersity effect[15] has a very small influence on the quantitative results of the reduced osmotic pressure.

Quite recently, Shiwa[3] utilized a slightly different renormalization group technique, viz., a cutoff method instead of the dimensional regularization scheme to calculate the osmotic compressibility for solutions of flexible polymers at good-solvent conditions. It may be noted that the theoretical models of Oono et al. and Shiwa are identical except for the detail of computation methods, which have different ways to treat higher order corrections. The analogous form for the reduced osmotic pressure in the model of Shiwa reads as[7]

$$(M/RT)(\Pi/c) = 1 + b\left[\frac{(1 + X_{(2)})^{(\epsilon/4)+2} - 1}{((\epsilon/4) + 2)X_{(2)}} - \frac{(1 + X_{(2)})^{(\epsilon/4)+1} - 1}{((\epsilon/4) + 1)X_{(2)}}\right] \quad (7)$$

where $b = \exp[(\epsilon/4)(1 + \ln 2)]$. In order to make a direct comparison possible, without any adjustable parameters, between the theoretical prediction and experimental results, Shiwa introduced[3] a scaled static variable of the form

$$X_{(2)} = 2cA_2M/b \quad (8)$$

We are now able to construct explicit functional forms for the entanglement parameter. However, before proceeding, let us first consider some problems associated with the first-order perturbation ϵ-expansion method. It has been revealed from a number of renormalization group studies[16-18] on polymers that the ϵ-expansion method with the first-order calculation on $\epsilon = 4 - d$ does not yield exact numerical results. In order to partially account for the higher order corrections of ϵ and to recover the correct scaling behavior in the asymptotic limit, a frequently used

augmentation procedure,[14,16,18,19] which improves the numerical results, will be adopted in this work. This augmentation is accomplished by substituting the factor $(\epsilon/4)$ by $A \equiv (2 - d\nu)/(d\nu - 1)$, where $d = 3$. The parameter ν is the excluded-volume exponent characterizing the molecular weight dependence of the radius of gyration. For flexible polymers at good-solvent conditions, ν assumes a value of 0.588 (the most accurate theoretical value).[20] Now we may recall that ΔF represents the excluded-volume interaction contribution of the free-energy density; hence, only the second term on the right-hand side of eqs 5, 5a, and 7 is relevant for the calculation of ΔF. Since Π/c is universal in $X_{(1)}$ or $X_{(2)}$ (cf. eqs 5 and 7) and $c \propto X_{(1)}$ or $X_{(2)}$ (cf. eqs 6 and 8), it is straightforward to write eq 4 in terms of $X_{(1)}$ or $X_{(2)}$. When eqs 2, 4, and 5 are combined, the entanglement parameter may be expressed as

$$\psi_{(1)} = (1/4)\int_0^{X_{(1)}} \exp\left\{A\frac{Z}{1+Z}\left[\frac{\mu^2}{X^2}\ln(\mu) + \left(1 - \frac{\mu^2}{X^2}\right)\ln(\mu + X) + \frac{\mu}{X}\right]\right\} dX \quad (9)$$

In the limit $Z \to \infty$ this relation simplifies as

$$\psi_{(1)} = (1/4)\int_0^{X_{(1)}} \exp\left\{A\left[\frac{\mu^2}{X^2}\ln(\mu) + \left(1 - \frac{\mu^2}{X^2}\right)\ln(\mu + X) + \frac{\mu}{X}\right]\right\} dX \quad (9a)$$

where $A = 0.3089$ at good-solvent conditions with $\nu = 0.588$. The integrals on the right-hand side of eqs 9 and 9a have in the present study been solved numerically with recourse to an algorithm of Romberg.

In a corresponding manner, the results of Shiwa may be written on the following analogous form:

$$\psi_{(2)} = (1/2)\int_0^{X_{(2)}} (b/X)\left[\frac{(1+X)^{A+2} - 1}{(A+2)X} - \frac{(1+X)^{A+1} - 1}{(A+1)X}\right] dX \quad (10)$$

The analytical result is[3]

$$\psi_{(2)} = (b/2)\left[\left(1 + \frac{1}{X_{(2)}}\right)\frac{(X_{(2)}+1)^{1+A} - 1}{1+A} - \frac{1}{X_{(2)}}\frac{(X_{(2)}+1)^{2+A} - 1}{2+A}\right] \quad (11)$$

Thus, with aid of eqs 9, 9a, and 11, we have outlined an approach to calculate, on an explicit form without any adjustable parameter, the ratio D_s/D_0 given by eq 1.

Figure 1 illustrates the X-dependence of ψ for the different theoretical approaches; viz., the curves designated (1)–(3) are calculated with the aid of eqs 9a (with $\mu = 1$ and $Z \to \infty$), 11, and 9 (with $\mu = 1$ and $Z = 0.1$), respectively. In order to be able to make a direct quantitative comparison between results from the different models (curves (1) and (2)), a scaled variable αX is constructed, with $\alpha = 1$ for curves (1) and (3) and $\alpha = 1.50$ for curve (2). The reason for this measure is that the ψ-values calculated from eqs 9a and 11, respectively, refer to different static overlap parameters (cf. eqs 6a and 8). We should note that the values of ψ calculated by means of eq 9a are approximately 15% higher than the corresponding ones evaluated from eq 11. In Figure 1 is also the effect of excluded-volume interactions on the entanglement parameter depicted (cf. curves (1) and (3)).

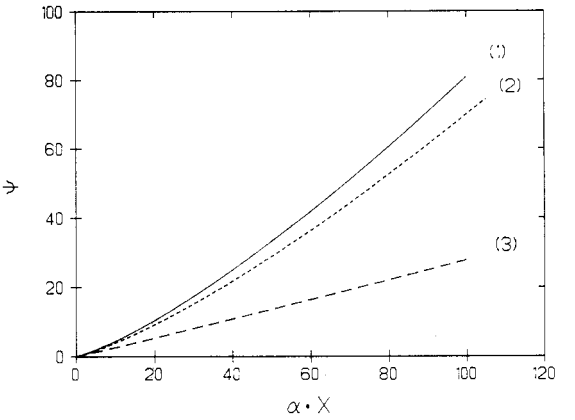

Figure 1. Entanglement parameter, calculated for different models, as a function of the scaled quantity αX, where $\alpha = 1$ for curves (1) and (3) and $\alpha = 1.50$ for curve (2) (cf. the main text). Curves (1)–(3) are evaluated from eq 9a with $Z \to \infty$, eq 11, and eq 9 with $Z = 0.1$, respectively.

Previously, it has been recognized[7] that reduced osmotic pressures evaluated from eq 5 are in somewhat better agreement with experimental values than those calculated from the theory of Shiwa (eq 7). Hence, an analogous trend can be anticipated to show up in a corresponding comparison of the behavior of ψ. Furthermore, eq 9 is more flexible than the formula of Shiwa because polydispersity effects of the polymer can be accounted for, and excluded-volume interactions of various strength may be simulated. In light of these considerations, we will in the next section on tracer diffusion express the results only in terms of the $\psi_{(1)}$ parameter.

Tracer Diffusion. In this section the diffusion transport of one tracer chain, D_t, with polymerization index n_t, in a matrix, where all matrix chains have the same polymerization index, n_m, is considered. We will briefly summarize some of the basic concepts and equations in the model of Hess.[11] The central theme of this theory is the competition between the lateral diffusion coefficients of the matrix, $D_m^{\perp}$, and the tracer, $D_t^{\perp}$, and the interplay between the longitudinal diffusion coefficients of the tracer, D_t'', and the matrix, D_m''. The final equation for D_t reads as

$$D_t = \frac{k_B T}{n_t\left(\zeta + (4/3)\dfrac{k_B T/n_c}{D_t'' + D_t^{\perp} + D_m'' + D_m^{\perp}}\right)} \quad (12)$$

The longitudinal diffusion coefficients are defined in the following way:

$$D_t'' = (1/3)\frac{k_B T}{n_t \zeta} \quad (13)$$

$$D_m'' = (1/3)\frac{k_B T}{n_m \zeta} \quad (14)$$

D_t'' and D_m'' represent the center-of-mass diffusion coefficients of a one-dimensional Rouse chain for the tracer and the matrix, respectively. The features of the lateral diffusion coefficient of the matrix may be expressed in the form

$$D_m^{\perp} = \begin{cases} (2/3)\dfrac{k_B T}{n_m \zeta}(1 - n_m/n_c) & \text{for } n_m \le n_c \\ 0 & \text{for } n_m \ge n_c \end{cases} \quad (15)$$

The quantity n_c, the critical polymerization index, is an

essential feature of the model and characterizes the crossover to a dynamical mode, in which the lateral motion on a global scale is completely blocked ($D_m^{\perp} = 0$; $n_m \geq n_c$) and the curvilinear motion or reptation is predominant.

When it comes to the lateral tracer diffusion coefficient, two different cases appear. For $n_m \geq n_c$ ($D_m^{\perp} = 0$), the following expression emerges:

$$D_t^{\perp} = \begin{cases} (2/3)\dfrac{k_B T}{n_t \zeta}(1 - 2n_t/n_c) & \text{for } n_t \leq n_c/2 \\ 0 & \text{for } n_t \geq n_c/2 \end{cases} \quad (16)$$

The disappearance of $D_t^{\perp}$ for large n_t indicates a transition to a dynamical state in which the lateral motion of the tracer freezes in and reptation-like dynamics is observed. In this case, in contrast with self-diffusion, the reptation transition of the "tagged" polymer occurs at a polymerization index that is only half of the critical polymerization index of the matrix. For $n_m \leq n_c$, the analogous relation can be written in the form

$$D_t^{\perp} = (1/3)\frac{k_B T}{n_t \zeta}\left\{1 - \frac{n_t}{n_c} - \frac{n_t}{n_m} + \left[\left(1 - \frac{n_t}{n_c} - \frac{n_t}{n_m}\right)^2 + 4\left(\frac{n_t}{n_m} - \frac{n_t}{n_c}\right)\right]^{1/2}\right\} \quad (17)$$

In this case no reptation transition of the tracer polymer chain is expected.

In this theory, n_c is of crucial significance for a self-consistent description of the various dynamical regimes. The critical segment number depends on the matrix concentration and may by analogy with eq 2 be related to the $X_{(1)}$-dependent function $\psi_{(1)}$ through

$$n_c = n_m/\psi_{(1)}(X_{(1)}) \quad (18)$$

This equation predicts that the critical chain length decreases with increasing matrix concentration.

Now we have the tools for the construction of expressions for the depiction of tracer diffusion under various conditions. When eqs 13–16 and 18 are inserted in eq 12, the following relationships are obtained for the case $n_m \geq n_c$ ($\psi_{(1)}(X_{(1)}) \geq 1$)

$$D_t/D_0 = \begin{cases} 1 - \dfrac{n_t \Psi_{(1)}}{n_m}\dfrac{4}{3 + n_t/n_m} & \text{for } \dfrac{n_t \Psi_{(1)}}{n_m} \leq 1/2 \quad (19a) \\ \dfrac{1}{1 + \dfrac{n_t \Psi_{(1)}}{n_m}\dfrac{4}{1 + n_t/n_m}} & \text{for } \dfrac{n_t \Psi_{(1)}}{n_m} \geq 1/2 \quad (19b) \end{cases}$$

Equation 19a represents a situation where the lateral motion of the matrix is blocked but the lateral mode of the tracer is only hindered. Equation 19b portrays a dynamical state where the lateral mobility of both tracer and matrix are frozen in. Substituting eqs 13–15, 17, and 18 in eq 12, we arrive at the following expression for $n_m \leq n_c$ ($0 \leq \psi_{(1)}(X_{(1)}) \leq 1$)

$$D_t/D_0 = 1/\left[1 + (n_t\psi_{(1)}/n_m)\left[4/\left[2 + 2\frac{n_t}{n_m} - 3\frac{n_t\psi_{(1)}}{n_m} + \left[\left(1 - \frac{n_t}{n_m} - \frac{n_t\psi_{(1)}}{n_m}\right)^2 + 4\left(\frac{n_t}{n_m} - \frac{n_t\psi_{(1)}}{n_m}\right)\right]^{1/2}\right]\right]\right] \quad (20)$$

In this case the lateral motions of both tracer and matrix are only hindered by interaction. Since n_c is related to the concentration or $X_{(1)}$-dependent parameter $\psi_{(1)}$, a progressive increase of the matrix concentration will sooner or later lead to a situation where n_c approaches n_m and $\psi_{(1)}(X_{(1)}) \to 1$. In this limit a transition to a different dynamic regime takes place ($n_m \geq n_c$) in which the tracer diffusion behavior is described by eqs 19a and/or 19b depending on whether or not the value of the parameter $n_t\psi_{(1)}/n_m$ is smaller or larger than $^1/_2$.

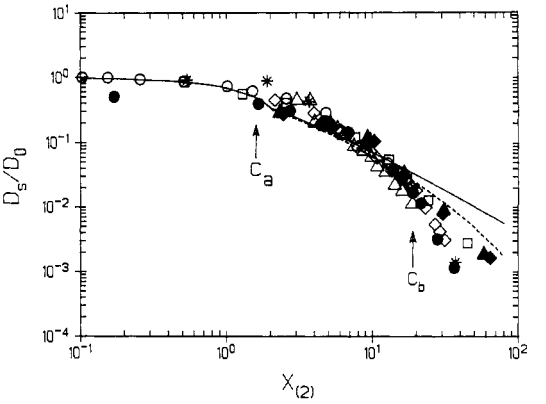

Figure 2. Reduced self-diffusion coefficient for polystyrene solutions under good-solvent conditions as a function of the scaled static variable $X_{(2)}$, which is calculated from eq 8. PS–benzene:[21] (○) $M = 7.83 \times 10^4$ (FRS); (□) $M = 7.54 \times 10^5$ (FRS). PS–perdeuteriobenzene:[55,56] (△) $M = 1.10 \times 10^5$ (PNMR); (◇) $M = 3.5 \times 10^5$ (PNMR); (●) $M = 1.10 \times 10^5$ (PNMR). PS–tetrahydrofuran:[29] (▲) $M = 4.98 \times 10^5$ (PNMR); (◆) $M = 1.05 \times 10^5$ (PNMR). PS–dibutyl phthalate:[57] (*) $M = 3.55 \times 10^5$ (FRS). The solid curve is calculated from eq 1 in combination with eq 11, with no adjustable parameters. The dashed curve represents the situation when the change in local effective friction with concentration is accounted for (cf. the main text). c_a and c_b indicate the transition from dilute to semidilute solution behavior and semidilute to concentrated solution behavior, respectively. The concentration variable and the static overlap parameter are numerically related through the following approximate relation: $X_{(2)} = 1.87 \times 10^{-2} M^{0.714} c$.

Results and Discussion

Self-Diffusion. Frequently used experimental techniques to measure self-diffusion in binary polymer solutions are forced Rayleigh light scattering (FRS)[21] and pulsed-field-gradient NMR (PNMR).[22]

In Figure 2 a large body of experimental self-diffusion data, representing both FRS and PNMR measurements of *polystyrene* over wide ranges of molecular weight and concentration, and at *good*-solvent conditions, are displayed on a log–log plot of the form D_s/D_0 versus $X_{(2)}$. The universal feature of the plot is reflected by the condensation of the experimental data points. Although, there is a scatter of the experimental points, this is not considered to be alarming since data obtained from these experimental techniques may, especially in the range of small values of D_s, be marred by relatively large errors (up to 40%); moreover, the results represent data from two different experimental techniques and from various research groups. The overlap threshold concentration, c_a, in Figure 2 (see also Figure 3) indicates the transition from dilute to semidilute solution behavior and is calculated from $c_a = 1.08/[\eta]$,[23] where $[\eta]$ is the intrinsic viscosity. The concentration designated as c_b marks the demarcation between the semidilute and the concentrated regime and is estimated from[24] $c_b = (0.77/[\eta])(R_{G,\Theta}/R_G)^{-8}$, where R_G and $R_{G,\Theta}$ are the radii of gyration in a good solvent and at Θ solvent conditions, respectively. The construction of the solid curve in Figure 2 is based on Hess theory (eq 1), incorporating the model of Shiwa (eq 11) for the calculation of $\psi_{(2)}$. In a broad outline the agreement between experimental results and the theoretical prediction is considered to be reasonable up to the concentrated regime. In the theoretical model of Hess the reptation transition

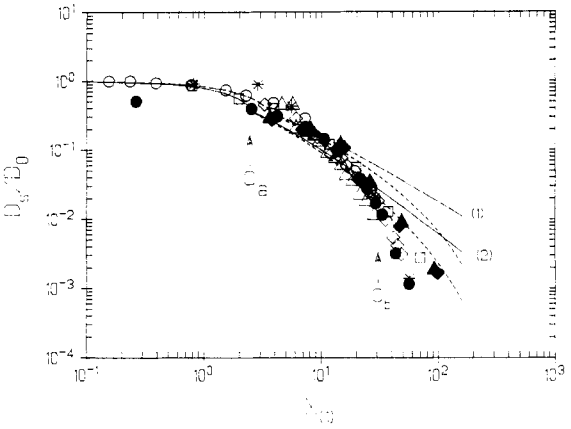

Figure 3. Reduced self-diffusion coefficient for polystyrene solutions as a function of the scaled static variable, $X_{(1)}$, which is calculated from eq 6. Symbols are the same as in Figure 2. Curve (1) is calculated from eq 1 in combination with eq 9 for $Z = 0.1$. Curve (2) represents eq 1 together with eq 9a for $Z \rightarrow \infty$. All calculations are carried out without any adjustable parameter. The dashed curves represent the friction-corrected counterparts of curves (1) and (2) (cf. the main text). c_a and c_b have the same meaning as in Figure 2. The concentration variable and the static overlap parameter are numerically related through the following approximate relation: $X_{(1)} = 2.88 \times 10^{-2} M^{0.714} c$.

is visually observed as a cusp of the curve, representing the switch over from eq 1a to eq 1b. Hess has remarked[10] that the sharpness of the reptation transition may be an artifact originating from neglect of coupling between center-of-mass motion and internal fluctuations in the segment distribution of the chains.

The somewhat peculiar crossover appearance in Figure 2 (as well as in other figures), in the form of a cusp may be an artifact due to redundant approximations.[10] However, it is possible that this crossover effect reflects an even more fundamental deficiency of the theoretical model. In search of a rational explanation of the departure between experimental results and theory in the transition region and for indication of possible modifications of the existing theoretical model, the following factors should be considered: (1) The model of Hess rests on the assumption that the hydrodynamic interactions are completely screened. However, there are evidences[2-4,6,25] that screening of both hydrodynamic and excluded-volume interactions in the semidilute range is a gradual process. If these trends are accounted for, the shape of the theoretical curve in the transition domain may change. (2) Global motions of chains are assumed to be uncorrelated, and coupling between the curvilinear and the lateral motions with respect to the local direction of the probe chain is treated as small. Similar conditions are invoked in the conventional "tube" picture, where reptative motion of vicinal chains is presumed to be entirely uncorrelated with motion of the probe chain. In this context it is interesting to note a recent theoretical study by Fixman,[26] who elaborated a modified reptation model in terms of correlated motion. In that approach the reptative motion of the test chain is always accompanied by correlated viscoelastic and reptative responses of matrix chains. If this type of coupled motion takes place in semidilute solutions, some of the assumptions introduced by Hess may be invalid. (3) In the present study a static scaling variable ($X_{(1)}$ or $X_{(2)}$) is engaged in the analysis of the results. Since self-diffusion is a dynamical process, it may be argued for a dynamic scaling variable. However, at the present stage we have not found an appropriate procedure to introduce such a parameter. Previous diffusion studies,[14,27] where the reduced mutual diffusion coefficient was plotted versus a scaling variable, have shown that a better agreement between the experimental data and the theoretical model is obtained if a dynamic parameter (k_{Dc}; the coefficient k_D expresses the first-order concentration dependence of the mutual diffusion coefficient) is chosen instead of a static one. In order to illustrate the impact of the choice of overlap parameter, we may note a recent work,[28] where self-diffusion data for polystyrene were analyzed with the aid of the Hess theory in combination with the model of Shiwa for the calculation of the entanglement function. A good concordance between the experimental data and the theoretical prediction was observed in the semidilute regime by treating the scaling variable as an adjustable parameter.

It has recently been argued[29,30] that one should account for the concentration dependence of the local effective monomer friction coefficient, ζ, in analyzing self-diffusion coefficients in the concentrated regime. It has been suggested[30] that the concentration dependence of the solvent diffusion coefficient may be used as an estimate of the changes in local effective friction. The following relation[31] is often utilized

$$D/D_{s,0} = (1 - \phi)/(1 + \phi)^2 \qquad (21)$$

where ϕ is the polymer volume fraction and $D_{s,0}$ and D are the solvent diffusion coefficients at polymer volume fraction zero and ϕ, respectively. This relationship has been shown[31] to describe the polymer concentration dependence of solvent diffusion for a number of polymer–solvent systems over a wide concentration range. It is assumed tha the relation $D/D_{s,0} \equiv \zeta_0/\zeta$, where ζ_0 is the local effective friction coefficient at infinite dilution, approximately holds. In light of this, the theoretical polymer self-diffusion coefficients in Figures 2 and 3 (see below) have been scaled by the ratio ζ/ζ_0; i.e., $((D_s/D_0)(\zeta_0/\zeta))$ is considered to account for the change in local effective friction with concentration (cf. dashed curve in Figure 2). The agreement between experimental data and the theoretical prediction is extended to higher concentrations, but still a significant divergence abides in the concentrated region. Before we proceed, it is important to emphasize that the theoretical model of Hess, as well as the approaches for the calculation of the entanglement parameter, is only designed to describe the physical behavior in polymer solutions covering the dilute and the "effective" semidilute regime. At higher concentrations, deviations between experimental results and theoretical predictions are not unexpected. Below, some of the complications that may arise in the theoretical description of the concentrated region will be indicated.

The renormalization group theory, which constitutes the basis for the evaluation of the entanglement parameter, incorporates the Edwards Hamiltonian extended to a many-chain system.[32] It has been established[14-19] that this Hamiltonian is a powerful theoretical tool in making good predictions for the static properties of polymers in semidilute solution. However, it is assumed that, for a strict validity of the Hamiltonian, in the description of the behavior of a polymer system, low total monomer density is required. In order to fulfill this prerequisite, it may be necessary to work with very long polymer chains, so that the "effective" semidilute solution behavior is attained at a relative low total polymer concentration. In this limit a plot of the reduced osmotic pressure ($\Pi M/RTc$) versus a static scaling variable is predicted to yield a universal curve. In the case of "ordinary" long polymer chains at finite concentration, a gradual deviation from the universal curve with increasing concentration has recently been

reported.[7] At concentrations of about 0.2 g/cm³ and for the molecular weight range represented by the present self-diffusion data, the theoretical value of the reduced osmotic pressure is estimated to be 10–15% lower than the corresponding experimental values. At higher concentrations (usually above 0.3 g/cm³), a dramatic departure from the universal curve, with a marked breakdown of the universality, has been observed[33,34] in plotting experimental osmotic pressure data in the form indicated above. This effect manifests itself[34] by systematic deviations of the experimental points from the universal curve. The tendency of departure is enhanced with increasing concentration and is also a function of the molecular weight of the polymer. The deviations from universality, due to the effect of finite monomer concentration, have been rationalized in terms of a modified interaction[34] Hamiltonian. From the analysis an analytical expression emerged, which was found to describe the divergences quantitatively well.

Let us now discuss the repercussions of these effects on the present self-diffusion results. Since the osmotic pressure and the entanglement parameter are directly related to each other, analogous effects will affect the calculation of ψ. Almost all the self-diffusion data represented in this study lie in the concentration interval 0–0.25 g/cm³. For the highest concentrations in this region, the calculated values of the entanglement parameter are expected to be underestimated by ca. 20% at most, hence favoring too high values of the calculated reduced self-diffusion coefficients (cf. the solid curve in Figure 2; see also Figure 3). However, this effect can only to a small extent explain the observed divergence between the experimental self-diffusion data and the theoretical prediction in the range of high values of the overlapping parameter. In light of these findings we may suspect that the dynamical constituents adapted in the model of Hess are insufficient in the description of self-diffusion behavior in the concentrated regime. In the dynamical model devised by Hess, the three-segment and higher order correlations are neglected. This approximation can probably not be justified in the concentrated region. Furthermore, the progressively developed Θ-like behavior in the concentrated range can not be accounted for in the model of Hess either. Another complication that may come into play is that indicated by Fixman,[26] namely, that the reptative mode of the probe chain may be strongly correlated to reptative motion of vicinal chains.

Figure 3 shows a comparison of the same experimental data as in Figure 2 with the theoretical prediction of Hess (eq 1), where $\psi_{(1)}$ now is calculated from eq 9 for the cases $\mu = 1$, $Z \to \infty$ (curve (2)) and $\mu = 1$, $Z = 0.1$ (curve (1)). A change of the polydispersity parameter, μ, has very little effect on the appearance of the theoretical curves. The main features of the prediction representing fully developed excluded-volume interactions (curve (2)), and its friction-corrected counterpart, are very similar to those depicted in Figure 2. It is expected that the effective thermodynamic conditions become poorer with increasing polymer concentration and that "Θ-like" conditions are developed in the concentrated regime. In order to mimic weak excluded-volume interactions, curve (1) is constructed. In the crossover region, between dilute and semidilute solution behavior, we note that the curve coincides well with the experimental data, but the agreement is poor at higher values of $X_{(1)}$.

Phillies[35,36] has recently demonstrated that an empirical equation, in the form of a stretched exponential, can successfully be fitted to experimental data describing the

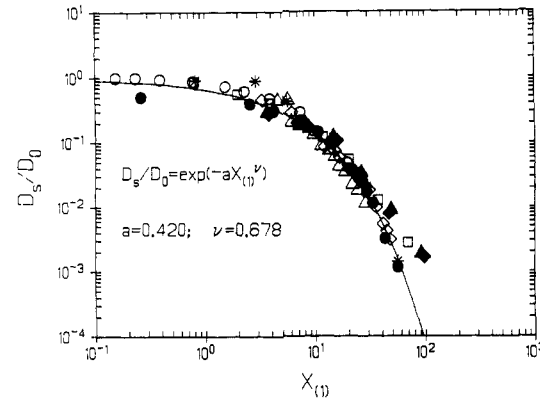

Figure 4. Reduced self-diffusion coefficient for polystyrene solutions under good-solvent conditions as a function of the scaled static variable, $X_{(1)}$, which is calculated from eq 6. Symbols are the same as in Figure 2. The solid curve is constructed from eq 22a with the aid of indicated values of the fitting parameters a and ν.

concentration dependence of the self-diffusion coefficient. The expression can be cast in the form

$$D_s/D_0 = \exp(-ac^{\nu}) \tag{22}$$

where a and ν are the fitting parameters. A normalized form may be obtained by rewriting the relation in terms of the reduced static variable $X_{(1)}$

$$D_s/D_0 = \exp(-a_1 X_{(1)}^{\nu_1}) \tag{22a}$$

Equation 22, as well as analogous functional forms[36,37] for sedimentation and viscosity, have been found to be powerful for an empirical description of experimental data for various polymer–solvent systems.

In Figure 4 the experimental self-diffusion data (the same as in Figures 2 and 3) are analyzed by using a non-linear least-squares fit of eq 22a to the data. A good fit, with $a_1 = 0.420$ and $\nu_1 = 0.678$, is obtained by allowing the parameters to float during the fitting procedure.

Recently, a heuristic derivation of eq 22 was presented,[38] yielding a value of $\nu = 1$ and $\nu = {}^1/_2$ for low and high molecular weights, respectively. In addition, a value of a of 2 was predicted[39] for a polystyrene sample with $M = 1.0 \times 10^6$ in a good solvent, while the best fit value to the experimental data was found to be 0.7. However, it has not been demonstrated unambiguously that the model has the ability to predict a priori values of both scaling variables a and ν, which, at the same time, are in quantitative agreement with those obtained from the fitting procedure of experimental data for a given system under specified conditions. It is possible that the success of eq 22 or 22a in analyzing self-diffusion data rather reflects the flexibility of the stretched exponential form than the intrinsic correctness of the underlying physical picture. It may be interesting to note that the form of eq 22 or 22a is reminiscent of the empirical Williams–Watts[40] relaxation function, $\gamma(t) = \exp[-(t/\tau)^{\beta}]$, where $0 < \beta \leq 1$ is a measure of the width of the distribution of relaxation times implied by the nonexponential character of the relaxation function, t is the experimental time, and τ is an effective decay time. The Williams–Watts model is, in conformity with the Phillies model, a two-parameter function, where β and τ are treated as fitting parameters. It is well-known that the W–W function is very flexible and frequently provides good fits to correlation function data, e.g., obtained from photon correlation spectroscopy, which exhibit a nonexponential decay.

Tracer Diffusion. In this section the concentration and molecular weight dependences of the tracer diffusion

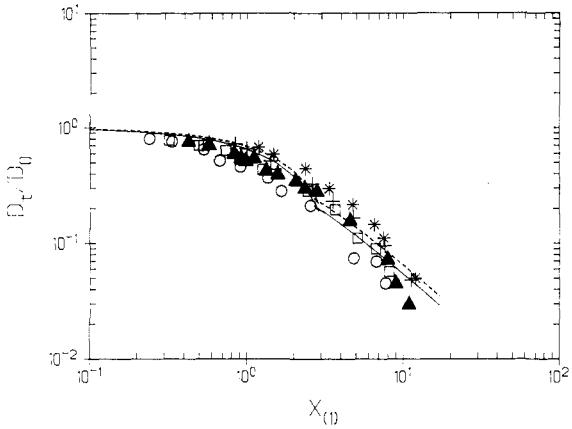

Figure 5. Reduced tracer diffusion coefficient for a high molecular weight polyisobutylene probe ($n_t = 8.7 \times 10^4$; $M_t = 4.9 \times 10^6$) in PIB–chloroform solutions[41] of various matrix molecular weights as a function of the static scaling variable, $X_{(1)}$, which is calculated from eq 6, with $A_2 = 1.49 \times 10^{-2} M^{-0.28}$ reported[58] for the system PIB–*n*-heptane: (○) $n_m = 1.43 \times 10^3$ ($m_m = 8.04 \times 10^4$); (□) $n_m = 3.24 \times 10^3$ ($M_m = 1.82 \times 10^5$); (▲) $n_m = 4.40 \times 10^3$ ($M_m = 2.47 \times 10^5$); (+) $n_m = 1.09 \times 10^4$ ($M_m = 6.10 \times 10^5$); (*) $n_m = 2.0 \times 10^4$ ($M_m = 1.1 \times 10^6$). Both curves are calculated from eq 20 in combination with eq 19b for the extreme cases ($n_t = 8.7 \times 10^4$; $n_m = 1.43 \times 10^3$) (solid curve) and ($n_t = 8.7 \times 10^4$; $n_m = 2.0 \times 10^4$) (dashed curve). All calculations are carried out without any adjustable parameter.

coefficient in homopolymeric solutions, as well as in ternary solutions of chemically different polymers, will be examined. Experimentally, the former situation has been studied[41] by utilizing dynamic light scattering (DLS) on a homopolymeric system, measuring the diffusion of a tracer chain of high molecular weight in solutions of a lower molecular weight component. The latter case is often realized by using the technique of DLS on isorefractive ternary solutions[30,42-45] of the type polymer 1–polymer 2–solvent. By this technique the tracer diffusion of a probe polymer, chosen for good optical contrast and compatibility, is monitored in refractive index-matched solutions containing an "invisible" background polymer and a suitable solvent.

Before discussing the results, we may recall the criteria that form the basis for the theoretical analysis of experimental tracer diffusion results. At sufficiently low matrix concentrations ($n_m \leq n_c$; $\psi_{(1)}(X_{(1)}) \leq 1$), eq 20 will be valid. As the matrix concentration increases, $\psi_{(1)}(X_{(1)})$ will gradually approach 1, and a transition to eq 19a and/or eq 19b, depending on whether the quantity $n_t\psi_{(1)}/n_m$ is smaller or larger than $^1/_2$, takes place.

In Figure 5 the behavior of the reduced tracer diffusion coefficient[41] of a high molecular weight ($M = 4.9 \times 10^6$) polyisobutylene (PIB) chain, in solutions of PIB of a lower molecular weight ($8 \times 10^4 \leq M \leq 1.1 \times 10^6$), is studied. This system fulfills well the prerequisites for which the original theoretical model of Hess[11] was elaborated. The theoretical curves, calculated from a combination of eqs 20 and 19b, represent the extreme cases $n_t = 8.73 \times 10^4$, $n_m = 1.43 \times 10^3$ (solid curve) and $n_t = 8.73 \times 10^4$, $n_m = 2.0 \times 10^4$ (dashed curve). The theoretical prediction is in fairly good agreement with the experimental result. By analogy with the self-diffusion case, the crossover to the reptation-like regime is observed in the form of a slight cusp of the curves. The weak molecular weight dependence as predicted by the theory can be traced in the experimental data.

The behavior of a ternary solution containing two chemically different polymers and a pure solvent is greatly affected by two thermodynamic factors, i.e., incompatibility

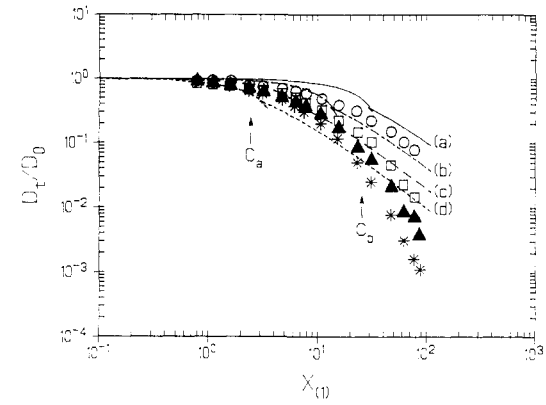

Figure 6. Reduced tracer diffusion coefficient of single PS chains of various molecular weights in solutions of PVME–*o*-fluorotoluene[49] with $n_m = 2.2 \times 10^4$ ($M_m = 1.3 \times 10^6$) as a function of the scaled static variable, $X_{(1)}$, which is calculated from eq 6, with $A_2 = 3.26 \times 10^{-3} M^{-0.171}$ determined from thermodynamic data reported[59] for the system PVME–2-butanone: (○) $n_t = 625$ ($M_t = 6.5 \times 10^4$); (□) $n_t = 1.72 \times 10^3$ ($M_t = 1.79 \times 10^5$); (▲) $n_t = 4.06 \times 10^3$ ($M_t = 4.22 \times 10^5$); (*) $n_t = 1.01 \times 10^4$ ($M_t = 1.05 \times 10^6$). The critical matrix concentrations, c_a and c_b, have the same meaning as in Figure 2. Curves (a)–(c) are all calculated from eq 20 in combination with eqs 19a and 19b for the cases $n_t = 625$, $n_m = 2.2 \times 10^4$; $n_t = 1.72 \times 10^3$, $n_m = 2.2 \times 10^4$; and $n_t = 4.06 \times 10^3$, $n_m = 2.2 \times 10^4$, respectively. Curve (d) is calculated from eq 20 in combination with eq 19b for the case $n_t = 1.01 \times 10^4$, $n_m = 2.2 \times 10^4$. All calculations are carried out without any adjustable parameter.

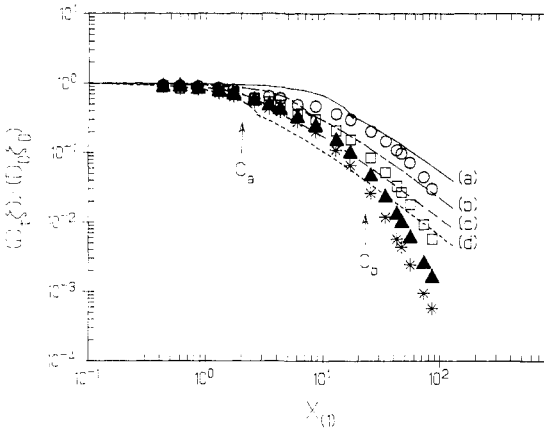

Figure 7. Normalized tracer diffusion coefficient of single PS chains of various molecular weights, corrected for changing local friction, in solutions of PVME–*o*-fluorotoluene[30] with $n_m = 1.1 \times 10^4$ ($M_m = 6.3 \times 10^5$) as a function of the scaled static variable, $X_{(1)}$, which is calculated from eq 6 with $A_2 = 3.26 \times 10^{-3} M^{-0.171}$ determined from thermodynamic data reported[59] for the system PVME–2-butanone. Symbols are the same as in Figure 6. The critical matrix concentrations, c_a and c_b, have the same meaning as in Figure 2. Curves (a)–(c) are all calculated from eq 20 in combination with eqs 19a and 19b for the cases $n_t = 625$, $n_m = 1.1 \times 10^4$; $n_t = 1.72 \times 10^3$, $n_m = 1.1 \times 10^4$; and $n_t = 4.06 \times 10^3$, $n_m = 1.1 \times 10^4$, respectively. Curve (d) is calculated from eq 20 in combination with eq 19b for the case $n_t = 1.01 \times 10^4$, $n_m = 1.1 \times 10^4$. All calculations are carried out without any adjustable parameter.

between the polymer components and solvent affinity to them.[46-48] In Figures 6–8 the concentration and molecular weight dependences of the reduced diffusion coefficient for tracer amounts of polystyrene (PS) of different molecular weights in solutions of poly(vinyl methyl ether) (PVME)–*o*-fluorotoluene,[30,49] with various molecular weights of the matrix polymer, are depicted. This system is expected[49,50] to be practically compatible. The reduced tracer diffusion coefficients in Figures 7 and 8 are scaled by the ratio ζ/ζ_0, to account for the change in the local monomer friction coefficient with increasing matrix

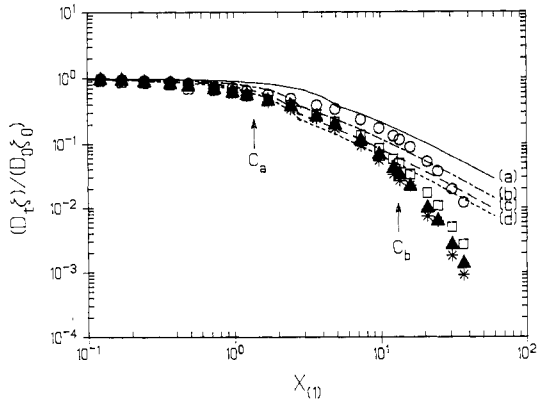

Figure 8. Normalized tracer diffusion coefficient of single PS chains of various molecular weights, corrected for changing local friction, in solutions of PVME–*o*-fluorotoluene[30] with $n_m = 2.4 \times 10^3$ ($M_m = 1.4 \times 10^5$) as a function of the static scaling variable, $X_{(1)}$, which is calculated from eq 6, with $A_2 = 3.26 \times 10^{-3} M^{-0.171}$ determined from thermodynamic data reported[59] for the system PVME–2-butanone. Symbols are the same as in Figure 6. The critical matrix concentrations, c_a and c_b, have the same meaning as in Figure 2. Curve (a) is calculated from eq 20 in combination with eqs 19a and 19b for the case $n_t = 625$, $n_m = 2.4 \times 10^3$. Curves (b)–(d) for all calculated from eq 20 in combination with eq 19b for the cases $n_t = 1.72 \times 10^3$, $n_m = 2.4 \times 10^3$; $n_t = 4.06 \times 10^3$, $n_m = 2.4 \times 10^3$; and $n_t = 1.01 \times 10^4$, $n_m = 2.4 \times 10^3$, respectively. All calculations are carried out without any adjustable parameter.

concentration. However, the main features observed in Figure 6, viz., the progressively stronger $X_{(1)}$ dependence of the reduced tracer diffusion coefficient in the region of high matrix concentrations and with increasing molecular weight of the optically labeled polymer, remain. In view of the various complications that may influence the results (cf. the discussion below), the theoretical predictions in Figures 6–8, as displayed by curves (a)–(d), may be considered to constitute a tentative description of the experimental results.

In search of a strict conformable experimental and theoretical picture, effects of the following type should be taken into account: (i) The same type of restrictions concerning static, dynamic, and concentration effects as those indicated in the discussion of self-diffusion results may, of course, also come into play in the interpretation of the tracer diffusion results. (ii) It has been suggested[30,49,51] that polystyrene coils undergo contraction upon the addition of matrix polymer and that a gradual transition from good to apparently Θ-like conditions occurs at fairly low concentration, before the coil overlap concentration is attained, of PVME. This kind of phenomenon will certainly make the theoretical analysis intricate. (iii) The PVME samples have been reported[30,49] to be rather polydisperse ($M_w/M_n \simeq 1.6$). Since this type of polydispersity effect is not accounted for in the model of Hess, the calculation of reduced tracer diffusion coefficients with the aid of eqs 19a, 19b, and 20 will probably not reproduce the actual situation. Furthermore, it is plausible that the dynamics of the probe chain may be sensitive to the length distribution of the matrix chains. Another disturbing factor is the question of the reliability of the "old" light-scattering data reported[59] for the system PVME–2-butanone. These data exhibit a big scatter of the experimental points when the second virial coefficient is plotted as a function of the molecular weight (these are to our knowledge the only light-scattering results available at present for PVME in solution). The polydispersity effect as well as possible large errors in the determination of A_2 may influence the magnitude of the value of the overlap variable and the entanglement parameter.

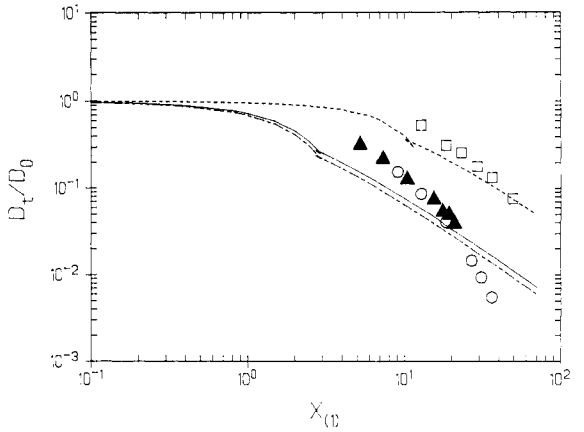

Figure 9. Reduced tracer diffusion coefficient of single PS chains in solutions of PMMA–benzene,[52] for different molecular weight combinations of tracer and matrix, as a function of the static scaling variable, $X_{(1)}$, which is calculated from eq 6, with $A_2 = 7.026 \times 10^{-3} M^{-0.261}$ reported[60] for the system PMMA–bromobenzene. The symbols have the following meaning: (○) $n_t = 8.10 \times 10^4$ ($M_t = 8.42 \times 10^6$) and $n_m = 4.05 \times 10^4$ ($M_m = 4.05 \times 10^6$); (▲) $n_t = 8.10 \times 10^4$ ($M_t = 8.42 \times 10^6$) and $n_m = 1.93 \times 10^4$ ($M_m = 1.93 \times 10^6$); (□) $n_t = 4.0 \times 10^3$ ($M_t = 4.2 \times 10^5$) and $n_m = 4.05 \times 10^4$ ($M_m = 4.05 \times 10^6$). The dashed curve (- - -) is calculated from eq 20 combined with eqs 19a and 19b for the case $n_t = 4.0 \times 10^3$, $n_m = 4.05 \times 10^4$. The two other curves are calculated from eq 20 in combination with eq 19b for the cases $n_t = 8.10 \times 10^4$, $n_m = 4.05 \times 10^4$ (—) and $n_t = 8.10 \times 10^4$, $n_m = 1.93 \times 10^4$ (– - –). All calculations are carried out without any adjustable parameter.

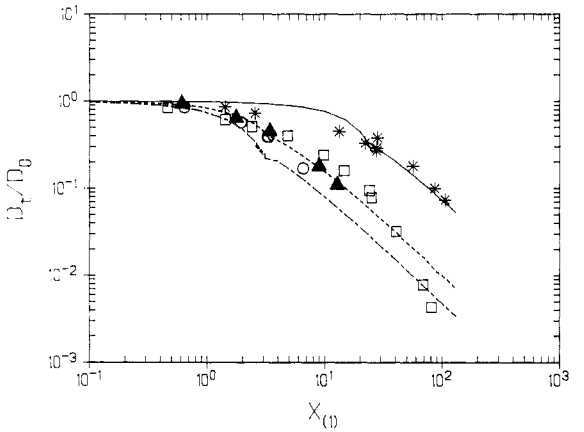

Figure 10. Reduced tracer diffusion coefficient of single PMMA chains in solutions of PS–thiophenol,[53] for a constant tracer molecular weight ($n_t = 3.42 \times 10^3$; $M_t = 3.42 \times 10^5$) and for different matrix molecular weights, as a function of the static scaling variable, $X_{(1)}$, which is calculated from eq 6, with $A_2 = 1.58 \times 10^{-2} M^{-0.286}$ reported[61] for the system PS–toluene: (○) $n_m = 422$ ($M_m = 4.39 \times 10^4$); (▲) $n_m = 1.79 \times 10^3$ ($M_m = 1.86 \times 10^5$); (□) $n_m = 7.45 \times 10^3$ ($M_m = 7.75 \times 10^5$); (*) $n_m = 8.10 \times 10^4$ ($M_m = 8.42 \times 10^6$). The curve (- - -) is calculated from eq 20 in combination with eq 19b for the case $n_t = 3.42 \times 10^3$, $n_m = 1.79 \times 10^3$. The two other curves are calculated from eq 20 in combination with eqs 19a and 19b for the cases $n_t = 3.42 \times 10^3$, $n_m = 7.45 \times 10^3$ (- - -) and $n_t = 3.42 \times 10^3$, $n_m = 8.10 \times 10^4$ (—). All calculations are carried out without any adjustable parameter.

Figure 9 shows a plot of D_t/D_0 versus $X_{(1)}$ for the slightly incompatible ternary system PS–poly(methyl methacrylate) (PMMA)–benzene,[52] in which the diffusion of single PS chains in isorefractive solutions of PMMA–benzene is monitored for various molecular weight combinations of guest (n_t) and host (n_m) polymers. The experimental data points from the two sets ($n_t = 8.10 \times 10^4$, $n_m = 1.93 \times 10^4$ and $n_t = 8.10 \times 10^4$, $n_m = 4.05 \times 10^4$) more or less collapse onto each other, whereas the other data set ($n_t = 4.0 \times 10^3$, $n_m = 4.05 \times 10^4$) exhibits a different appearance. These findings are in substance consistent with the theoretical

predictions (cf. the displayed curves). A more detailed comparison between theory and experimental results is unfortunately obstructed by the rather restricted concentration interval covered by these data.

In Figure 10 the concentration and molecular weight dependences of D_t/D_0 for a similar ternary system, PMMA–PS–thiophenol,[53] are illustrated. The diffusion of a single PMMA chain of a fixed molecular weight ($n_t = 3.42 \times 10^3$) in isorefractive solutions of PS–thiophenol is studied for different molecular weights of the matrix. The solvent thiophenol is considered[53,54] to be of the same quality for PMMA and PS as benzene or toluene. The tracer diffusion data for solutions of the three lowest matrix molecular weights ($n_m = 422$, 1.79×10^3, and 7.45×10^3) apparently do not deviate from each other in a systematic way, whereas the data for the high molecular weight sample ($n_m = 8.10 \times 10^4$) display a different pattern of behavior. The theoretical predictions coincide, on the whole, with the experimental findings.

Conclusions

In this paper, models, based on results from renormalization group methods for the entanglement parameter in combination with the theoretical approach of Hess, to analyze self-diffusion and tracer diffusion behavior in polymer solutions in terms of a static scaling variable, are scrutinized. From the models, explicit analytical functions, without any adjustable parameter, for the description of self-diffusion and tracer diffusion in polymer solutions are developed.

A large body of experimental self-diffusion data is found to condense in a unified manner, when the reduced self-diffusion coefficient is plotted versus a static overlap parameter. The experimental self-diffusion data are in a broad outline described by the theoretical model.

In comparison of the concentration and molecular weight dependences of the experimental tracer diffusion coefficient, for different polymeric systems of various incompatibility, with theoretical predictions, a broadly consistent picture appears.

The peculiar shape of the theoretical curve for the description of the transition domain to semidilute behavior, as well as the observed gradual deviation between experimental self-diffusion data and theory in the concentrated regime, is attributed to deficiencies of the theoretical models.

Acknowledgment. We thank Professor Y. Oono for helpful correspondences. Financial support from the Norwegian Research Council for Science and the Humanities (NAVF) is gratefully acknowledged.

References and Notes

(1) de Gennes, P.-G. *Scaling Concepts in Polymer Physics*; Cornell University Press: Ithaca, NY, 1979.
(2) Doi, M.; Edwards, S. F. *The Theory of Polymer Dynamics*; Oxford University Press: Oxford, 1986.
(3) Shiwa, Y. *Phys. Rev. Lett.* **1987**, *58*, 2102.
(4) Shiwa, Y.; Oono, Y.; Baldwin, P. R. *Macromolecules* **1988**, *21*, 208.
(5) Nyström, B.; Waernes, Ø.; Roots, J. *J. Polym. Sci., Polym. Lett. Ed.* **1989**, *27*, 271.
(6) Nyström, B.; Roots, J. *J. Polym. Sci., Polym. Phys. Ed.* **1990**, *28*, 521.
(7) Nyström, B.; Roots, J. *J. Polym. Sci., Polym. Lett. Ed.* **1990**, *28*, 101.
(8) de Gennes, P.-G.; Léger, L. *Annu. Rev. Phys. Chem.* **1982**, *33*, 49.
(9) Léger, L.; Viovy, J. L. *Contemp. Phys.* **1988**, *29*, 579.
(10) Hess, W. *Macromolecules* **1986**, *19*, 1395.
(11) Hess, W. *Macromolecules* **1987**, *20*, 2587.
(12) Skolnick, J.; Yaris, R.; Kolinski, A. *J. Chem. Phys.* **1988**, *88*, 1407.
(13) Schweizer, K. S. *J. Chem. Phys.* **1989**, *91*, 5802.
(14) Oono, Y.; Baldwin, P. R. *Phys. Rev. A* **1986**, *33*, 3391.
(15) Ohta, T.; Oono, Y. *Phys. Lett.* **1982**, *89A*, 460.
(16) Oono, Y. *Adv. Chem. Phys.* **1985**, *61*, 301.
(17) Freed, K. F. *Renormalization Group Theory of Macromolecules*; Wiley-Interscience: New York, 1987.
(18) Cherayil, B. J.; Bawendi, M. G.; Miyake, A.; Freed, K. F. *Macromolecules* **1986**, *19*, 2770.
(19) Nakanishi, A.; Ohta, T. *J. Phys. A* **1985**, *18*, 127.
(20) Le Guillou, J. C.; Zinn-Justin, J. *Phys. Rev. Lett.* **1977**, *39*, 95.
(21) Léger, L.; Hervet, H.; Rondelez, F. *Macromolecules* **1981**, *14*, 1732.
(22) Callaghan, P. T.; Pinder, D. N. *Macromolecules* **1980**, *13*, 1085.
(23) Utracki, L.; Simha, R. *J. Polym. Sci., Part A* **1963**, *1*, 1089.
(24) Graessley, W. W. *Polymer* **1980**, *21*, 258.
(25) Muthukumar, M.; Edwards, S. F. *Polymer* **1982**, *23*, 345.
(26) Fixman, M. *J. Chem. Phys.* **1988**, *89*, 3892.
(27) Wiltzius, P.; Haller, H. R.; Cannell, D. S.; Schaefer, D. W. *Phys. Rev. Lett.* **1984**, *53*, 834.
(28) Pinder, D. N. *Macromolecules* **1990**, *23*, 1724.
(29) von Meerwall, E. D.; Amis, E. J.; Ferry, J. D. *Macromolecules* **1985**, *18*, 260.
(30) Wheeler, L. M.; Lodge, T. P. *Macromolecules* **1989**, *22*, 3399.
(31) Blum, F. D.; Pickup, S.; Foster, K. R. *J. Colloid Interface Sci.* **1986**, *113*, 336.
(32) Edwards, S. F. *Proc. Phys. Soc.* **1965**, *85*, 613.
(33) Oono, Y., private communication.
(34) Baldwin, P. Thesis, 1987.
(35) Phillies, G. D. J. *Macromolecules* **1986**, *19*, 2367.
(36) Phillies, G. D. J. *J. Phys. Chem.* **1989**, *93*, 5029.
(37) Phillies, G. D. J.; Peczak, P. *Macromolecules* **1988**, *21*, 214.
(38) Phillies, G. D. J. *Macromolecules* **1987**, *20*, 558.
(39) Phillies, G. D. J. *Macromolecules* **1988**, *21*, 3101.
(40) Williams, G.; Watts, D. C. *Trans. Faraday Soc.* **1970**, *66*, 80.
(41) Brown, W.; Pu, Z. *Macromolecules* **1989**, *22*, 3508; **1989**, *22*, 4031.
(42) Hadgraft, J.; Hyde, A. J.; Richards, R. W. *J. Chem. Soc., Faraday Trans. 2*, **1979**, *75*, 1495.
(43) Martin, J. E. *Macromolecules* **1984**, *17*, 1279.
(44) Numasawa, N.; Hamada, T.; Nose, T. *J. Polym. Sci., Polym. Phys. Ed.* **1986**, *24*, 19.
(45) Borsali, R.; Duval, M.; Benmouna, M. *Macromolecules* **1989**, *22*, 816.
(46) van den Esker, M. W. J.; Vrij, A. *J. Polym. Sci., Polym. Phys. Ed.* **1976**, *14*, 1943.
(47) Broseta, D.; Leiber, L.; Joanny, J.-F. *Macromolecules* **1987**, *20*, 1935.
(48) Tong, Z.; Einaga, Y.; Kitagawa, T.; Fujita, H. *Macromolecules* **1989**, *22*, 450.
(49) Wheeler, L. M.; Lodge, T. P.; Hanley, B.; Tirrell, M. *Macromolecules* **1987**, *20*, 1120.
(50) Cotts, D. B. *J. Polym. Sci., Polym. Phys. Ed.* **1983**, *21*, 1381.
(51) Chang, T.; Han, C. C.; Wheeler, L. M.; Lodge, T. P. *Macromolecules* **1988**, *21*, 1870.
(52) Numasawa, N.; Kuwamoto, K.; Nose, T. *Macromolecules* **1986**, *19*, 2593.
(53) Nemoto, N.; Inoue, T.; Makita, Y.; Tsumashima, Y.; Kurata, M. *Macromolecules* **1985**, *18*, 2516.
(54) Nemoto, N.; Inoue, T.; Tsumashima, Y.; Kurata, M. *Bull. Inst. Chem. Res., Kyoto Univ.* **1984**, *62*, 177.
(55) Callaghan, P. T.; Pinder, D. N. *Macromolecules* **1984**, *17*, 431.
(56) Fleisher, G.; Zgadzoi, O. E.; Skirda, V. D.; Maklakov, A. I. *Colloid Polym. Sci.* **1988**, *266*, 201.
(57) Inoue, T.; Nemoto, N.; Kojima, T.; Kurata, M. *Polym. J. (Tokyo)* **1988**, *20*, 869.
(58) Cervenka, A.; Marek, M.; Solc, K.; Kratochvil, P. *Collect. Czech. Chem. Commun.* **1968**, *33*, 4248.
(59) Manson, J. A.; Arquette, G. J. *Makromol. Chem.* **1960**, *37*, 187.
(60) Su, A. C.; Fried, J. R. *Macromolecules* **1986**, *19*, 1417.
(61) Varma, B. K.; Fujita, Y.; Takahashi, M.; Nose, T. *J. Polym. Sci., Polym. Phys. Ed.* **1984**, *22*, 1781.

Registry No. Polystyrene, 9003-53-6.